

## Post-Assembly Functionalization of Supramolecular Nanostructures with Bioactive Peptides and Fluorescent Proteins by Native Chemical Ligation

Sahir Khan,<sup>†,‡,§</sup> Shantanu Sur,<sup>†</sup> Patricia Y. W. Dankers,<sup>†</sup> Ricardo M. P. da Silva,<sup>†</sup> Job Boekhoven,<sup>†,¶</sup> Taylor A. Poor,<sup>§,||</sup> and Samuel I. Stupp\*,<sup>†,||,¶,¶</sup>

<sup>†</sup>Institute for BioNanotechnology in Medicine, Northwestern University 303 East Superior Avenue, Rm. 11-123, Chicago, Illinois 60611, United States

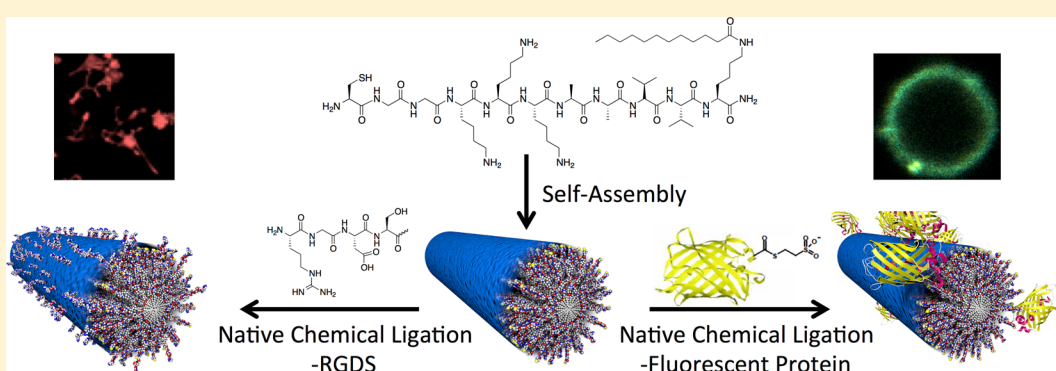
<sup>‡</sup>Department of Biomedical Engineering, <sup>§</sup>Department of Molecular Biosciences, and <sup>¶</sup>Department of Chemistry, Northwestern University Tech Building, 2145 Sheridan Avenue, Evanston, Illinois 60208, United States

<sup>||</sup>Medical Scientist Training Program, Feinberg School of Medicine, Morton Building, R. 1-670, 303 East Chicago Avenue, Chicago, Illinois 60611, United States

<sup>¶</sup>Department of Materials Science and Engineering, Northwestern University Cook Hall, Rm. 1-3002, 2220 Campus Drive, Evanston, Illinois 60208, United States

<sup>¶</sup>Department of Medicine, Feinberg School of Medicine Galter Pavilion, Suite 3-150, 251 East Huron Street, Chicago, Illinois 60611, United States

### Supporting Information



**ABSTRACT:** Post-assembly functionalization of supramolecular nanostructures has the potential to expand the range of their applications. We report here the use of the chemoselective native chemical ligation (NCL) reaction to functionalize self-assembled peptide amphiphile (PA) nanofibers. This strategy can be used to incorporate specific bioactivity on the nanofibers, and as a model, we demonstrate functionalization with the RGDS peptide following self-assembly. Incorporation of bioactivity is verified by the observation of characteristic changes in fibroblast morphology following NCL-mediated attachment of the signal to PA nanofibers. The NCL reaction does not alter the PA nanofiber morphology, and biotinylated RGDS peptide was found to be accessible on the nanofiber surface after ligation for binding with streptavidin-conjugated gold nanoparticles. In order to show that this strategy is not limited to short peptides, we utilized NCL to conjugate yellow fluorescent protein and/or cyan fluorescent protein to self-assembled PA nanofibers. Förster resonance energy transfer and fluorescence anisotropy measurements are consistent with the immobilization of the protein on the PA nanofibers. The change in electrophoretic mobility of the protein upon conjugation with PA molecules confirmed the formation of a covalent linkage. NCL-mediated attachment of bioactive peptides and proteins to self-assembled PA nanofibers allows the independent control of self-assembly and bioactivity while retaining the biodegradable peptide structure of the PA molecule and thus can be useful in tailoring design of biomaterials.

## INTRODUCTION

A biomaterial developed as an artificial extracellular matrix (ECM) mimic must recapitulate several features of the native ECM. The nanoscale surface features<sup>1</sup> and mechanical properties<sup>2</sup> of the scaffold should be tuned for the targeted

Received: October 29, 2013

Revised: March 5, 2014

Published: March 26, 2014

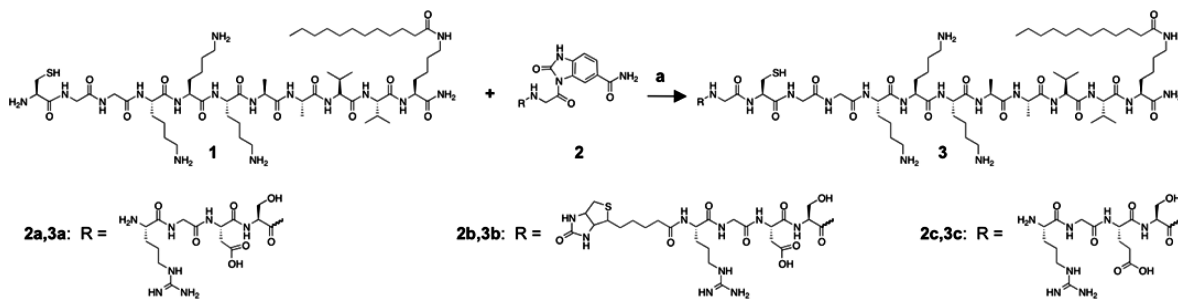


**Figure 1.** NCL reaction scheme. The reaction mixture containing 1 mM CysPA (**1**), 1 mM peptide-Nbz (**2**), 5 mM 4-MPAA, and 5 mM DTT in PBS was reacted at pH 7.4 for 24 h at 37 °C to generate peptide-functionalized PA (**3**). The peptides used in the reaction are RGDS (**2a,3a**), biotin-RGDS (**2b,3b**), and RGES (**2c,3c**).

tissue in order to achieve precise control of cellular behavior.<sup>3</sup> The chemical structure of the biomaterial should ideally contain chemical bonds that allow biodegradation *in vivo* and thus eventually be replaced by native ECM.<sup>4</sup> Finally, the method for incorporating biological functionality into the material should be applicable to a broad array of bioactive molecules, from small molecules to peptides to proteins.

Biomaterials based on peptide amphiphiles (PAs) meet many of these criteria. PA molecules, composed of an oligopeptide conjugated to a lipid tail, self-assemble into supramolecular nanostructures.<sup>5</sup> The chemical structure of the PA molecule does not contain any non-natural components or linkages, and PA nanostructures are biodegradable and biocompatible *in vivo*.<sup>6</sup> Our group pioneered the use of peptide sequences that lead to the self-assembly of high aspect ratio cylindrical nanofibers and at the same time effectively display bioactive cues on their surfaces.<sup>7</sup> This self-assembly process is mediated by hydrophobic collapse of the lipid tails and  $\beta$ -sheet formation among oligopeptides.<sup>8</sup> The highly entangled PA nanofiber gel mimics the fibrillar nature of native ECM<sup>9b</sup> and confers tunable mechanical rigidity and supramolecular cohesiveness.<sup>9</sup> Biological activity is provided by inclusion of bioactive peptide sequences that can bind soluble ligands or cell surface receptors.<sup>10</sup> The presentation of multiple bioactive cues on a single PA nanofiber at high surface densities<sup>11</sup> that maximize signaling capability can be achieved through coassembly of different PA molecules.<sup>12</sup> Through the inclusion of different bioactive cues, PA nanofibers have demonstrated the capacity to signal for differentiation,<sup>13</sup> proliferation,<sup>14</sup> biological adhesion,<sup>15</sup> angiogenesis,<sup>16</sup> and insulin secretion.<sup>17</sup> Previous strategies to incorporate bioactivity into PA nanostructures have generally been limited to short peptide sequences that allow for the solid-phase peptide synthesis of the entire PA molecule, including the bioactive sequence. However, the presence of a bioactive cue can potentially influence the self-assembly process of the PA molecules, resulting in the formation of an altered nanostructure.<sup>18</sup> Post-assembly functionalization of the PA nanostructures with bioactive groups would allow independent control of self-assembly and incorporation of bioactivity. Furthermore, in many cases the complexity of ligand–receptor binding interactions cannot be fully recapitulated with short peptides. The ability to attach larger peptides and proteins to the self-assembled PA nanostructure would therefore expand the scope of possible biological applications.

One approach for conjugating larger peptides and proteins to the self-assembled PA nanostructure is native chemical ligation (NCL). Originally developed by Dawson et al. in 1994, NCL

achieves the chemoselective formation of a native peptide bond between peptides or protein fragments.<sup>19</sup> This reaction occurs at neutral pH upon simple mixing of two reactive precursors, one containing an N-terminal cysteine residue and the other containing a C-terminal thioester moiety.<sup>20</sup> In contrast with conjugation strategies such as carbodiimide-mediated amide chemistry or Schiff base formation, amine-containing lysine residues and carboxylic acid-containing glutamate and aspartate residues do not interfere with the NCL reaction. Moreover, the NCL reaction occurs under biocompatible conditions, unlike other chemoselective conjugation strategies such as copper-catalyzed click chemistry.<sup>21</sup> In the context of peptide-based self-assembled systems, the NCL reaction has been utilized to enhance the mechanical strength of a hydrogel composed of fibrillar  $\beta$ -sheet peptides via terminal cross-linking<sup>22</sup> and for surface PEGylation of self-assembled monolayers.<sup>23</sup> The biocompatibility of the NCL reaction has been demonstrated by its use in a FRET-based probe for *in vivo* cellular imaging<sup>24</sup> and by its use for cross-linking soluble polymers into hydrogels for three-dimensional cell culture.<sup>25</sup> In addition, the NCL reaction has been used to conjugate relatively large bioactive moieties, including proteins and other macromolecules.<sup>26</sup>

In this work, we investigate the use of post-assembly modification of PA nanostructures using NCL as an approach to add bioactivity while retaining the basic one-dimensional morphology. As a model, our objective has been to carry out functionalization of fibers with the fibronectin derived epitope RGDS<sup>27</sup> as a bioactive cue. We have also investigated the attachment of proteins to the fibers using thioester-terminated fluorescent proteins.

## RESULTS AND DISCUSSION

**NCL Conjugation of RGDS Peptide to the Surface of PA Nanofibers.** The NCL reaction was used to conjugate peptides functionalized with an N-acyl-benzimidazolinone leaving group at the carboxy terminus<sup>20</sup> (peptide-Nbz, **2**) to PA molecules functionalized with a cysteine residue at the amino terminus (CysPA, **1**). Both components were synthesized using standard Fmoc-protected solid phase peptide synthesis with commercially available resins. The NCL reaction was performed upon simple mixing of reactants in the presence of a mild reducing agent (DTT) and thiol catalyst (4-MPAA) in PBS at pH 7.4 (Figure 1). This reaction occurs via a three-step mechanism,<sup>19a</sup> with initial substitution of the peptide-Nbz leaving group with the thiol catalyst to form a thioester, followed by attack from the free thiol group of the cysteine on the CysPA, and finally an irreversible intramolecular rearrangement that generates the native peptide bond (SI Figure 1a).

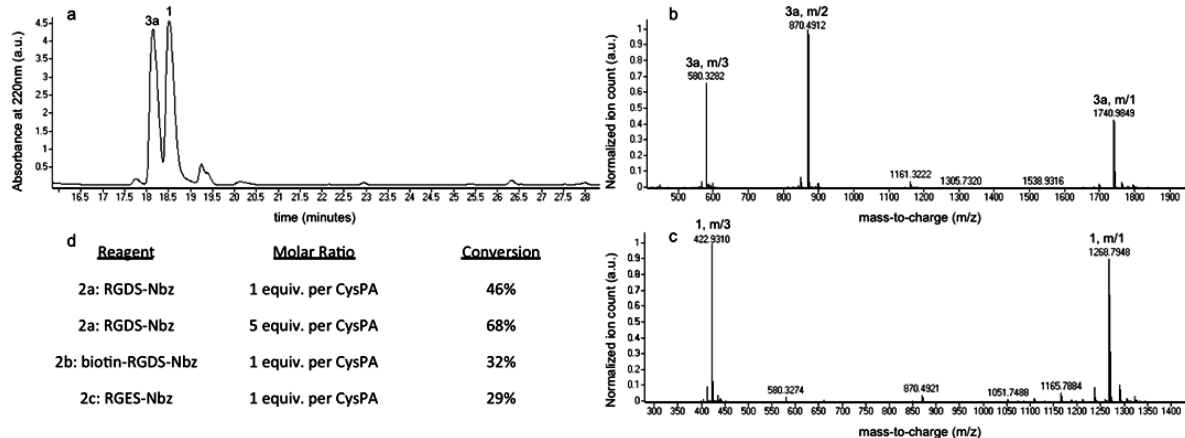


**Figure 2.** Reaction yields and analysis. (a) LCMS trace of NCL reaction between RGDS peptide and CysPA. (b,c) The two major peaks correspond to the RGDS-PA product 3a (b) and residual CysPA 1 (c). (d) The percent conversion of the CysPA was calculated based on integration of the peaks for multiple NCL reactions.

This mechanism was confirmed by observing the presence of the thioester intermediate 4 in the mass spectrum of the NCL reaction at 3 h (SI Figure 1b).

The solution-phase NCL reaction was analyzed by liquid chromatography with electrospray ionization mass spectrometry (LC-MS). A 1:1 mixture of the two reactants generated the desired product (RGDS-PA, 3a) that was separable from the CysPA (Figure 2a). Two major peaks identified in the mass spectra were the CysPA 1 and the RGDS-PA product 3a (Figure 2b,c). Based on integration of the major peaks, the NCL reaction proceeded to 46% conversion of the CysPA. Similar analyses on NCL reactions with different reagent mixtures are shown in Figure 2d. Increasing the concentration of the RGDS-Nbz to a 5-fold excess increased the conversion to 68%. We hypothesize that the proximity of the reactive cysteine residues on the surface of the CysPA nanofibers creates steric limitations preventing the reaction from achieving quantitative conversion of all reactive sites. However, complete conversion of reactive sites is not necessary to achieve optimal bioactivity, as we demonstrate below.

The self-assembled nanostructures that the CysPA formed were analyzed before and after the NCL reaction using negatively stained transmission electron microscopy (TEM). The CysPA self-assembled in aqueous solution into high aspect ratio nanofibers of approximately 10 nm diameters with a variable degree of bundling, and this morphology was conserved following the NCL reaction (Figure 3a and b). The secondary structure within the nanofibers was investigated using CD spectroscopy (SI Figure 2). The CD spectra of the CysPA before and after the NCL reaction with RGDS-Nbz peptide suggested a mixture of  $\beta$ -sheet and random coil secondary structure (estimated by fitting to linear combinations of reference spectra) with a minimal change caused by the conjugation of epitope. Interestingly, the spectra from presynthesized RGDS-PA had a predominant  $\alpha$ -helical character. This result indicates that the presence of epitope on the PA molecule could influence the self-assembly process and the resulting secondary structure.

To confirm that the ligated peptide is present on the surface of the PA nanofiber, we added a biotin group to the N-terminus of the RGDS-Nbz peptide (biotin-RGDS-Nbz, 2b) and used NCL to attach this peptide to the CysPA nanofiber. Labeling the reaction product (biotin-RGDS-PA, 3b) with 10 nm

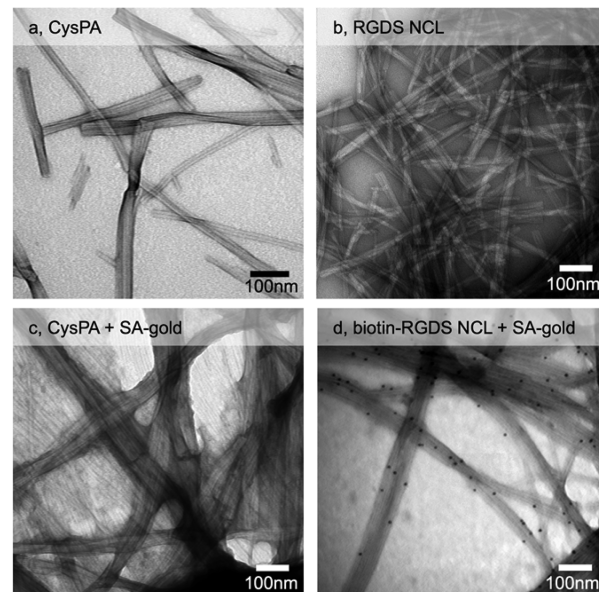


**Figure 3.** Surface accessibility of NCL-conjugated PA assemblies. (a,b) TEM micrograph of CysPA (a) and NCL RGDS-PA (b) negatively stained with uranyl acetate. (c,d) TEM micrographs of NCL RGDS-PA (c) and NCL biotin-RGDS-PA (d) following incubation with streptavidin-conjugated gold nanoparticles (SA-gold).

streptavidin-conjugated gold nanoparticles (SA-gold) confirmed the ligation and accessibility of biotin-RGDS peptide on the nanofiber surface (Figure 3d). The SA-gold did not bind to CysPA nanofibers reacted with nonbiotinylated RGDS peptide (Figure 3c). This result also demonstrates another potential strategy for incorporation of bioactivity, as the accessible biotin moiety can be utilized for further functionalization of the PA surface with avidin-conjugated bioactive molecules.

**Cellular Response to RGDS-Ligated Nanofibers.** The binding of SA-gold to biotin-RGDS-conjugated nanofibers confirmed the accessibility of the NCL-conjugated peptides on the nanofiber surface. We next investigated whether such post-assembly peptide conjugation could be used to deliver ECM signals to cells. Since fibroblasts are extensively studied in the context of RGDS presenting scaffold materials,<sup>15,28</sup> we used these cells to test the bioactivity of NCL-modified PA

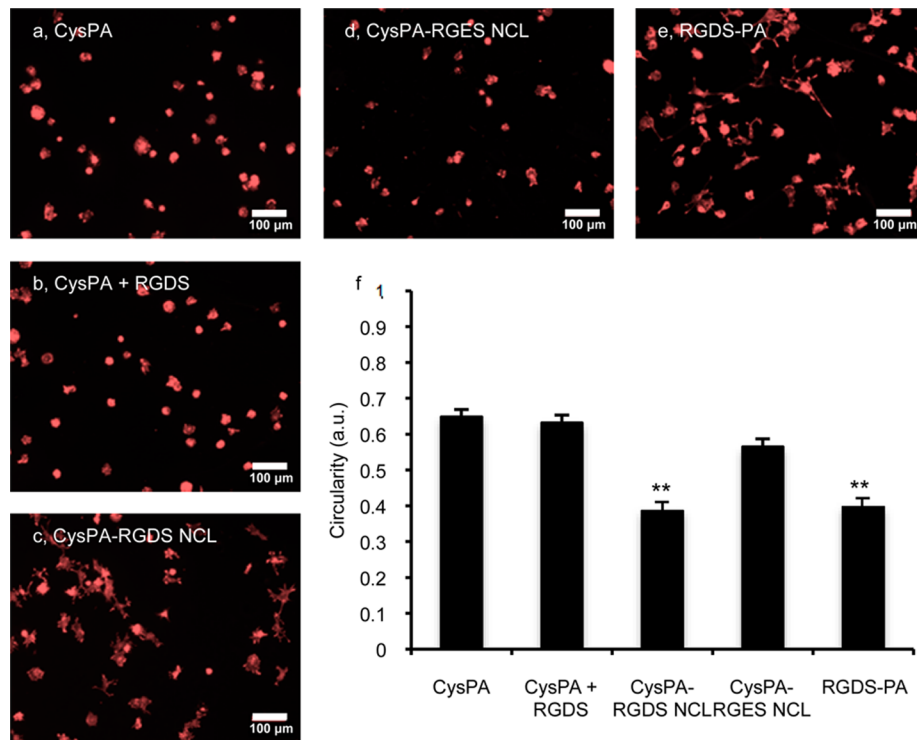


**Figure 4.** Fibroblast morphology on PA-coated coverslips. (a–e) Fluorescent micrographs of NIH/3T3 fibroblasts cultured for 5 h and stained by phalloidin for F-actin on coverslips coated with CysPA (a), CysPA and soluble RGDS peptide (b), NCL RGDS-PA (c), NCL RGES-PA (d), and presynthesized RGDS-PA not formed by NCL (e). (f) Comparison of cell circularity ( $4\pi \times \text{area}/\text{perimeter}^2$ ) on various PA-coated surfaces (\*\*  $p < 0.01$  vs CysPA,  $n = 100$  cells).

nanofibers. Cell response was measured to PAs coated on glass coverslips using a method previously established in our group.<sup>29</sup> Sterile coverslips were first coated with cationic poly(D-lysine) (PDL) and subsequently with a layer of anionic alginate, and finally with the cationic PA nanofibers (SI Figure 3). Not only does this method of sequential coating help to achieve a uniform PA layer on the surface, but the intermediate nonfouling alginate layer also prevents any confounding cell response resulting from attachment to underlying glass or PDL. NIH/3T3 mouse embryonic fibroblasts were seeded on these PA-coated surfaces and maintained under serum-free conditions to minimize nonspecific adsorption of proteins to the nanofibers.<sup>30</sup>

Fibroblast morphology was evaluated after 5 h of culture, as such short incubation was found to be suitable by our group and others for comparison of their response to substrates.<sup>28,29,31</sup> Fibroblasts were found to attach to CysPA surfaces but displayed a rounded morphology indicating a lack of cell spreading and adhesion (Figure 4a). This observation can be explained by the ability of PA nanofibers to provide cell attachment; however, an absence of an integrin-binding cue limits their spreading. In contrast, on the CysPA surfaces functionalized with the RGDS peptide using the NCL reaction (NCL RGDS-PA), cells appeared to be more spread with the presence of prominent cytoplasmic processes giving the cells a stellate morphology, similar to that found on presynthesized RGDS-PA (Figure 4c,e). The observed change in cell morphology was further quantified by measurement of circularity, calculated as  $4\pi \times \text{area}/\text{perimeter}^2$  so that a perfectly round cell will have a value of 1.<sup>32</sup> The circularity of fibroblasts on the NCL RGDS-PA surface was  $0.38 \pm 0.03$ , significantly lower than the value of  $0.65 \pm 0.04$  found on the CysPA surface

(Figure 4f). Cell viability was found to be higher than 95% in each of these conditions (SI Figure 4), indicating that a toxic response to the underlying substrate is not attributable to the difference in the cell morphology. To further evaluate whether the observed change in the cell morphology was specific to the RGDS sequence, we conjugated a mutated non-bioactive RGES peptide to CysPA nanofibers using the NCL reaction (NCL RGES-PA). Fibroblasts on the NCL RGES-PA surface (Figure 4d) had a circularity of  $0.56 \pm 0.04$ , which was not significantly different from the circularity on the CysPA surface, indicating that the change in cell morphology is due to the specific bioactivity of the RGDS peptide and not due to the conditions of the NCL reaction. Furthermore, addition of soluble RGDS peptide into the culture medium did not alter the morphology of cells on the CysPA surface (Figure 4b), confirming the need for tethering of the RGDS peptide to nanofibers to provide for cell signaling.

Although NCL did not achieve full conjugation efficiency, several reports from our group and others have shown that the presence of 10% bioactive molecules in a peptide nanofiber system is sufficient to demonstrate the maximal cell response.<sup>15,22</sup> Consistent with those findings, we observed a comparable cell response between the NCL RGDS-PA surfaces and the presynthesized RGDS-PA surfaces, which have a cue present on every molecule. It has been suggested that the critical RGD sequence density required for fibroblast spreading is determined by the steric factor separating two integrin molecules.<sup>33</sup> Even with a submaximal functionalization, following NCL reaction, RGDS sequence availability on the nanofiber surface would be sufficient for maximal integrin binding.

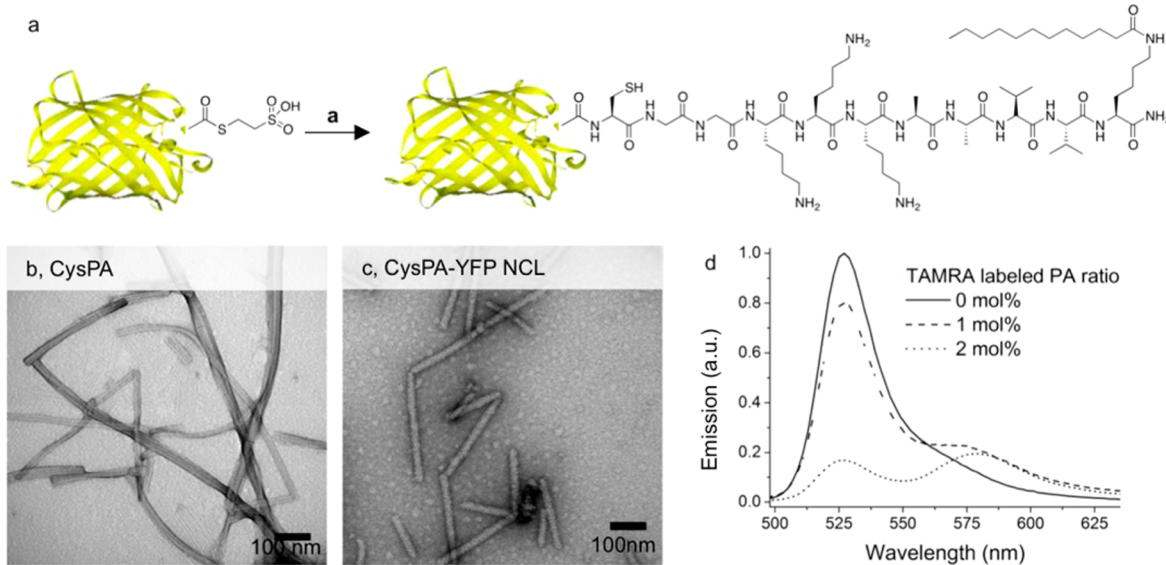


**Figure 5.** Protein ligation to PA nanostructures via NCL. (a) Schematic of NCL conjugation of YFP to CysPA using YFP-MESNA. (b,c) TEM micrograph of CysPA assemblies prior to (b) and following NCL with YFP (c). (d) Emission spectra of YFP following NCL conjugation to CysPA coassembled with different concentrations of TAMRA-labeled PA.

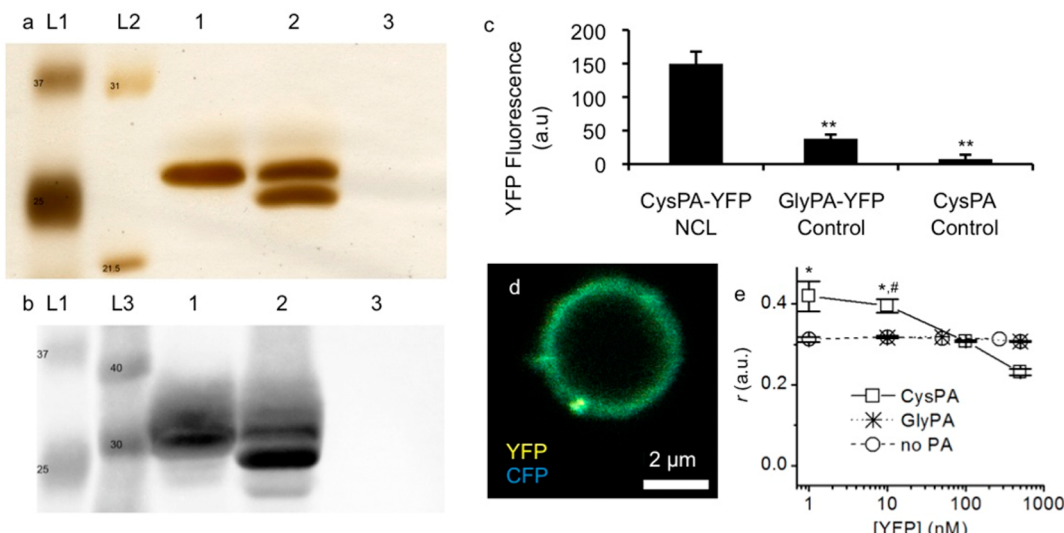


**Figure 6.** Characterization of PA–protein conjugates formed by NCL. (a,b) SDS-PAGE visualized by silver staining (a) and Western blot against GFP (b) were used to analyze the NCL reaction between YFP and PA (Lane 1: YFP only, Lane 2: YFP conjugated to CysPA, Lane 3: CysPA only, Lanes L1, L2, L3: protein standards with indicated molecular weights in kDa). (c) YFP fluorescence intensity after conjugation to CysPA-coated surface (CysPA-YFP NCL). An identical PA lacking cysteine (GlyPA-YFP Control) or CysPA treated with reaction buffer alone (CysPA Control) was used as a control (\*\*  $p < 0.01$  vs CysPA-YFP NCL). (d) Confocal fluorescence microscopy of CysPA nanofiber-coated alginate microparticles simultaneously reacted with YFP and CFP. (e) Fluorescence anisotropy of YFP following NCL reaction with CysPA. GlyPA was used as a control (\*  $p < 0.05$  vs YFP; #  $p < 0.05$  vs GlyPA).

Apart from the possibility of post-assembly functionalization of PA nanofibers, the NCL conjugation strategy allows simultaneous covalent functionalization of the PA nanofiber with multiple different bioactive ligands. This approach could take advantage of potential synergies among different classes of bioactive ligands without the need for independent chemical conjugation schemes for each component. Furthermore, the relative biocompatibility of the NCL reaction mixture creates the opportunity for temporal control over ligand conjugation in live cell culture, potentially allowing the sequentially timed presentation of bioactive cues to influence cell behaviors such as differentiation.

**Protein Ligation to PA Nanofibers in Solution and on Coated Surfaces.** Next, we sought to extend the scope of the NCL method for biofunctionalization of PA nanofibers to larger molecules such as proteins. To demonstrate that the NCL reaction can be used to ligate proteins to the PA nanofiber, we utilized YFP that was expressed with a self-cleavable intein domain and purified with 2-mercaptoethane sulfonate sodium salt (MESNA) to yield a thioester at the C-terminus. This YFP-MESNA was ligated to the CysPA via NCL with dilute reactant concentrations (Figure 5a). The overall nanofiber morphology of the CysPA was retained following conjugation with YFP, although the nanofibers appear wider

and less bundled (Figure 5b,c). These changes would be expected upon ligation of large proteins onto the nanofiber surface.

The CysPA-YFP NCL reaction mixture was analyzed by SDS-PAGE to identify the reaction product. Two distinct bands were detected on silver staining, one corresponding to the YFP and a second for a product that appears to have higher electrophoretic mobility than the YFP (Figure 6a). Western blot analysis showed both bands to be positively stained with anti-GFP antibody (Figure 6b). We attribute the band with higher electrophoretic mobility to YFP conjugated with PA; although conventionally, the electrophoretic mobility would be expected to decrease following conjugation due to an increase in molecular mass, we believe the character of the PA molecule to be responsible for the increased electrophoretic mobility. The conjugation of the PA molecule adds a highly hydrophobic aliphatic chain and three positively charged lysine residues to the YFP protein, and due to this aliphatic chain and these positive charges, the PA molecule can potentially bind a higher number of SDS molecules relative to its molecular mass than the protein alone, resulting in an increase in surface charge that is disproportionately higher than the increase in mass. This “gel shifting” effect has been observed for other proteins modified with hydrophobic groups,<sup>34</sup> as well as other peptide amphiphile systems<sup>35</sup> analyzed by electrophoresis with SDS. This effect would increase the apparent electrophoretic mobility of the product on SDS-PAGE, consistent with the new band observed in the reaction mixture. The possibility of the second band being a YFP degradation product can be excluded because the YFP control was treated under exactly the same conditions as the NCL reaction except for the absence of PA. Taken together, the new band observed in the reaction mixture likely corresponds to the CysPA-YFP ligation product.

In order to confirm the YFP immobilization on the CysPA nanofibers, we performed FRET experiments. The CysPA was coassembled with TAMRA-labeled PA (SI Figure 3a), which has an excitation spectrum that overlaps the YFP emission spectrum, forming a FRET pair. The proximity of YFP to TAMRA fluorophores on the nanofiber surface should therefore induce FRET and quench the YFP emission. For distances in the range of the Förster radius, closer proximity of the fluorophores will induce a greater degree of YFP emission quenching. This effect was observed as shown in Figure 5d, where all spectra were normalized using the maximum intensity observed in the absence of TAMRA (YFP emission maximum at 525 nm). Increasing the molar concentration of the TAMRA-labeled PA increases the surface density of acceptors. A higher density of TAMRA on the nanofiber surface effectively reduces the average distance from YFP attached via NCL, resulting in greater quenching. In fact, increasing the proportion of TAMRA-labeled PA from 1 to 2 mol % generated an increase in the quenching of YFP fluorescence from 20% to 80%. For single donor–acceptor FRET pairs, the decrease in intensity of the donor is accompanied by an increase in intensity of the acceptor. However, at 2 mol % TAMRA fluorophore density on the nanofiber surface was high enough to induce self-quenching due to homo-FRET phenomena. Consequently, we did not observe an increased intensity of TAMRA signal with increasing energy transfer between YFP and TAMRA-PA.

The specificity of YFP immobilization on CysPA nanofibers via NCL was further confirmed by fluorescence anisotropy ( $r$ ) measurements. In the absence of depolarization phenomena,

such as homo-FRET, light scattering, or reabsorption, the anisotropy only depends on the rotational diffusion of the fluorophore. If the rotational diffusion rate of a fluorophore is of similar magnitude to the fluorescence decay rate, the slower rotational diffusion rate expected upon binding will be reflected as an increase in anisotropy. As shown in Figure 6e, at less than 10 nM, YFP anisotropy increased after NCL with CysPA but remained essentially the same in the presence of an identical PA lacking the N-terminal cysteine (GlyPA). Interestingly, the anisotropy decreased steadily as the concentration increased above a threshold of 10 nM YFP. At higher concentration of YFP, the likelihood for the distance between two or more YFP molecules to be shorter than the Förster radius for homo-FRET can no longer be neglected. Therefore, the anisotropy decreases due to energy transfer between fluorophores with different orientations. A similar behavior was observed previously for YFP-labeled protein homodimers and used to detect protein reorientation upon binding.<sup>36</sup> These results provide evidence not only that the YFP was immobilized on the CysPA nanofibers by NCL, but also that the surface density of immobilized YFP increased as the YFP to CysPA molar ratio increased in the reaction mixture.

Finally, we sought to demonstrate that protein ligation via NCL can be achieved on PA nanofiber-coated surfaces. Higher fluorescence intensity was observed following the NCL-mediated conjugation of YFP to CysPA nanofibers coated on glass coverslips (Figure 6c). Conversely, adding the same YFP-containing reaction mixture to an identical PA lacking the N-terminal cysteine (GlyPA) produced significantly lower fluorescence intensity, indicating that the observed fluorescence was due to retention of the YFP by a specific reaction with CysPA and not a nonspecific adsorption to PA nanofibers. To demonstrate a potential application of protein ligation to PA nanofiber-coated surfaces via NCL, we utilized cell-size alginate microparticles electrostatically conjugated with a coating of CysPA nanofibers by a process similar to the formation of the CysPA-coated glass coverslips. We simultaneously ligated YFP and cyan fluorescent protein (CFP) to the surfaces of these CysPA-coated microparticles and visualized their surface fluorescence by confocal microscopy. The surfaces of the microparticles showed colocalized YFP and CFP fluorescence (Figure 5d), indicating that the two proteins were coligated to the PA-coated microparticles. A full view of the field shows separate areas of high intensity for each fluorophore, indicating that colocalization of fluorescence was not due to spectral bleed-through (SI Figure 3d).

The approach of conjugating proteins to PA nanofibers by NCL as described here can be applied to any protein expressed with a C-terminal intein domain and purified by thiol-mediated cleavage. The conjugated protein can potentially fulfill multiple functions, including targeting, adhesion, and cell signaling. These functions are especially useful when combined with the advantages offered by PA nanofibers, including the ability to encapsulate hydrophobic drugs, form a scaffold that mimics ECM, and coat polymer surfaces. For example, PA nanofibers encapsulating therapeutic agents<sup>37</sup> or drug loaded alginate particles coated with PA nanofibers could be targeted to specific cells and tissues via proteins conjugated by NCL. The conjugation of proteins to PA nanofibers via NCL would facilitate these potential applications while maintaining the desirable properties of biodegradability and biocompatibility inherent to the PA molecule.

## CONCLUSIONS

We have demonstrated here the use of native chemical ligation to conjugate both bioactive peptides and fluorescent proteins to self-assembled peptide amphiphile nanofibers. The ligated peptides and proteins were displayed on the nanofiber surface without compromising the morphology of the supramolecular nanostructures. Evidence for bioactivity was established by the observation of fibroblast spreading following conjugation of a biological signal to nanofibers using the ligation reaction. Our results suggest that post-assembly chemical ligation could be a useful tool to tailor the bioactivity of supramolecular nanostructures.

## EXPERIMENTAL PROCEDURES

**Peptide Synthesis and Purification.** All PAs and peptides were synthesized by fluorenylmethoxycarbonyl (Fmoc) protected solid-phase peptide synthesis as previously reported by our group<sup>7a</sup> using materials purchased from EMD Chemicals Inc. (Merck KGaA, Darmstadt, Germany) unless otherwise indicated. Briefly, the PAs were synthesized at 0.25 mmol scale on Rink Amide MBHA resin, and peptides functionalized at the carboxy-terminus with an N-acyl-benzimidazolinone for native chemical ligation (peptide-Nbz) were synthesized at 0.25 mmol scale on 3-(Fmoc-amino)-4-aminobenzoyl AM resin. For each amino acid addition, the resin was deprotected using 2% 1,8-diazabicycloundec-7-ene (DBU) and 2% piperidine in *N,N*-dimethylformamide (DMF), and the amino acid was coupled using 4 equiv of protected amino acid functionalized with 4 equiv of 2-(1-henzotriazole-1-yl)-1,3,3-tetramethyluronium hexafluorophosphate (HBTU) and 6 equiv of *N,N*-diisopropylethylamine (DIPEA) in DMF. The dodecanoic acid tail was similarly functionalized and coupled to a lysine side chain following selective deprotection of the 4-methyltrityl (Mtt) group using a 92:5:3 mixture of dichloromethane (DCM), triisopropylsilane (TIPS), and trifluoroacetic acid (TFA). For synthesis of peptide-Nbz, a Boc-protected amino acid was added at the N-terminus, and the resin was treated with 5 equiv *p*-nitrophenylchloroformate in DCM followed by 0.5 M DIPEA in DMF for activation. Resin cleavage and amino acid deprotection was performed using a 95:2.5:2.5 mixture of TFA, TIPS, and water for all PAs and peptides. Following removal of solvent by rotary evaporation, the crude PAs/peptides were precipitated by addition of cold diethyl ether. The precipitate was collected and dried *in vacuo* to generate crude product with identity confirmed by electrospray ionization (ESI) mass spectrometry. All PAs and peptides were purified by reverse-phase high performance liquid chromatography (HPLC) as previously reported by our group.<sup>7a</sup> Briefly, the crude product was dissolved in 0.1% TFA in water, filtered, injected onto a Gemini-NX 5 μm C18 column, and eluted using a water-acetonitrile solvent gradient for separation. The purified product was lyophilized and stored at -20 °C. To conjugate biotin, 10 mM RGDS-Nbz peptide in PBS was mixed 1:1 with 20 mM sulfo-NHS-biotin (Thermo Scientific, Rockford, IL) in PBS and reacted for 4 h at room temperature and overnight at 4 °C. The biotinylated peptide was purified from the reaction mixture by HPLC, lyophilized, and stored at -20 °C.

**Protein Expression and Purification.** The pTXB1-EYFP and pTXB1-ECFP plasmids (see Supporting Information) were transformed, according to the manufacturer's protocol, into *E. coli* BL21 (DE3) (Novagen) competent cells by electro-

poration.<sup>38</sup> The transformed cells were plated on Lysogeny Broth (LB)-agar plates containing ampicillin (Amp) and grown overnight at 37 °C. Single colonies were picked and grown in 30 mL LB medium (10 g peptone, 5 g yeast extract, 10 g sodium chloride, 1 L water) containing Amp overnight at 37 °C in shaker at 250 rpm. Cells were stored in 1 mL aliquots at -80 °C in the presence of 15% (w/v) glycerol. For overnight cultures, 10 mL of Amp-containing LB was inoculated with ~1 μL of the glycerol stock and grown overnight at 37 °C and 250 rpm. For small-scale expression, volumes of 30 mL were used, while large-scale expression was performed in 500 mL LB medium. Cell culturing was started with 5 mL overnight culture and cells were grown at 37 °C, 250 rpm in the presence of Amp. When an optical density (OD<sub>600</sub>) of 0.6–0.8 was reached, protein expression was induced by the addition of isopropyl-β-D-thiogalactopyranoside (IPTG; Duchefa Biochemie). Large-scale expression was induced by 0.5 mM IPTG and grown overnight at 15 °C. Cell harvesting was performed by centrifuging the cell culture for 5 min at 10,000 g at 4 °C. The supernatant was removed and the cell pellet was resuspended in 5 mL Bugbuster (Novagen) and 5 μL benzonase (Novagen) per gram of cell pellet. After incubation for 20 min at 21 °C, the cell suspension was centrifuged at 16,000 g for 20 min at 4 °C. The supernatant was directly applied to 10 mL chitin beads (New England Biolabs), equilibrated with 10 column volumes of column buffer (20 mM sodium phosphate, 0.5 M sodium chloride, pH 6). The loaded column was washed with 10 volumes of column buffer after which the column was quickly flushed with 2 column volumes of cleavage buffer (20 mM sodium phosphate, 0.5 M sodium chloride, 100 mM 2-mercaptoethane sulfonic acid (MESNA), pH 6). Subsequently, the flow was stopped and the column with the cleavage buffer was incubated 2 × 20 h at room temperature (using fresh cleavage buffer for the second time). Elution fractions containing the cleaved proteins with a C-terminal thioester were collected and pooled. The proteins were buffer-exchanged (into 20 mM Tris, 150 mM sodium chloride, pH 7.8) using Amicon ultra centrifuge tubes (MWCO: 10 kDa), after which the concentration was measured using UV-vis. Protein solutions were stored at -80 °C.

**Native Chemical Ligation Reaction in Solution.** The N-terminal cysteine PA (CysPA) was mixed with 5 equiv of dithiothreitol (DTT) and dissolved in phosphate-buffered saline (PBS) at pH 7.4, and the peptide-Nbz or YFP-MESNA was mixed with 5 equiv of 4-mercaptophenylacetic acid (4-MPAA) and dissolved in PBS at pH 7.4. The two reagents were mixed at the desired ratio, and the reaction was subsequently analyzed by liquid chromatography mass spectrometry, gel electrophoresis, transmission electron microscopy, circular dichroism (CD) spectroscopy, Förster resonance energy transfer (FRET), or fluorescence anisotropy as indicated.

**Liquid Chromatography Mass Spectroscopy.** Analytical liquid chromatography mass spectroscopy (LC-MS) was performed using an Agilent 1200 system with an Agilent 6250 quadrupole-time-of-flight mass spectrometer using a Phenomenex Gemini C18 column (5 μm particle size, 150 × 1.0 mm) eluting with a gradient of 5% ACN to 95% ACN in water, with each solvent containing 0.1% TFA. UV absorbance was monitored at 220 nm.

**Transmission Electron Microscopy.** The nanostructure morphology of each PA was characterized using conventional transmission electron microscopy (TEM). Each PA or NCL

reaction mixture was diluted in water to 0.1 mM PA, and 7.5  $\mu$ L of this solution was deposited on a copper grid with 300 mesh carbon support film for 5 min, washed with water twice for 1 min each, negatively stained with 2% (w/v) uranyl acetate twice for 30 s each, and dried at room temperature overnight.

For labeling, streptavidin-conjugated 10 nm gold nanoparticles in suspension (Sigma-Aldrich, St. Louis, MO) were mixed at 1:1 volume ratio with 20 mM dithiothreitol (DTT) in PBS and incubated for 30 min to prevent nonspecific thiol binding to the gold. This suspension was mixed at a 1:4 volume ratio with the PA or NCL reaction mixture and incubated for 30 min to allow streptavidin binding to biotin. This mixture was diluted to 0.1 mM PA and deposited onto the copper grid as described above, except with four water washes to ensure complete removal of unbound gold nanoparticles. All images were acquired using an FEI Tecnai Spirit G2 microscope working at 120 kV.

**Circular Dichroism Spectroscopy.** Circular dichroism (CD) spectra of PA (1 mM) in PBS or NCL reaction mixture were acquired on a JASCO J-715 CD spectrophotometer at room temperature using quartz plates with a 0.05 mm path length. The CD spectra were fit to linear combinations of reference spectra for known secondary structures using the PEPFIT algorithm<sup>39</sup> to estimate secondary structure.

**Gel Electrophoresis and Western Blotting.** Polyacrylamide gel electrophoresis with sodium dodecyl sulfate (SDS-PAGE) was performed using 17.5% polyacrylamide gels. Samples were prepared in SDS sample buffer with 4 M urea and heated for 5 min at 95 °C. The reaction mixture and controls were diluted 15-fold resulting in consistent protein loadings of approximately 5.6  $\mu$ g per well for the YFP and 0.5  $\mu$ g per well for the CysPA across all samples. As reference, Bio-Rad Precision Plus Unstained Protein Standard was used for both silver stain and Western blot, while Bio-Rad Broad-Range 15% Protein Standard was used specifically for the silver stain and Magic Mark XP Western Protein Standard (Invitrogen) was used specifically for the Western blot. Electrophoresis was performed at 65 V for 21 h in Tris-Glycine running buffer using the Pharmacia EPS 600 power supply. Gels were rinsed with water and developed by either silver nitrate exposure or Western blot. For the Western blot, the protein was transferred to an immobilin-P membrane using a Bio-Rad Trans-Blot cell with model 200/2.0 power supply at 35 V for 2 h in Tris-Glycine transfer buffer. The membrane was blocked using 5% milk in PBS + 0.3% Tween for 1 h. The membrane was then stained with anti-GFP rabbit polyclonal primary antibody (ab290, Abcam) at 1:5000 dilution for 1 h, washed with PBS + 0.3% Tween, further stained with goat anti-rabbit polyclonal secondary antibody conjugated to FITC (Jackson ImmunoResearch) at 1:5000 dilution for 1 h, and washed again with PBS + 0.3% Tween. The membrane was then read on a Fujifilm FLA-5100 imager.

**Förster Resonance Energy Transfer and Fluorescence Anisotropy.** CysPA was mixed in hexafluoroisopropanol (HFIP) with 5-carboxytetramethylrhodamine (TAMRA)-labeled PA at different ratios (0, 1, and 2 mol %) and lyophilized to ensure homogeneous mixing of coassembled nanofibers. The lyophilized powder was redissolved in 10 mM DTT aqueous solution, diluted in PBS at pH 7.4, and subsequently mixed with YFP-MESNA solution (supplemented with 5 equiv 4-MPAA), to yield final concentrations of YFP and PA of 1 and 100  $\mu$ M, respectively. This mixture was reacted for around 24 h before measurements. TAMRA was used as a FRET acceptor for YFP.

The same procedure was used to prepare solutions of an identical PA lacking the N-terminal cysteine (GlyPA). These solutions were used as control to rule out the contribution to FRET signal of potential nonspecific adsorption of YFP to PA nanofibers. Emission intensity spectra were recorded on a Horiba Nanolog fluorimeter, using an excitation wavelength of 485 nm (bandpass of 2 nm). Emission intensity was scanned between 495 and 680 nm (increment of 1 nm), encompassing both YFP and TAMRA emission ranges, using a bandpass of 2 nm, integration time of 0.1 s, and PMT detector set at 950 kV. A similar procedure was used to prepare solutions for fluorescence anisotropy (FA), but without TAMRA labeled PA, and at variable YFP concentration (1–500 nM). FA was recorded at an emission wavelength of 535 nm (excitation at 495 nm), 1 s integration time, and using variable monochromators' bandpasses, which were set to guarantee signal intensities over 10 kCPS. Intensity was recorded at the four possible combinations for the orientations of excitation and emission polarizers: both along the vertical direction ( $I_{VV}$ ), both oriented horizontally ( $I_{HH}$ ), the excitation polarizer oriented vertically and the emission horizontally ( $I_{VH}$ ), or vice versa ( $I_{HV}$ ). FA ( $r$ ) was calculated according to the following equation:

$$r = (I_{VV} \cdot I_{HH} - I_{VH} \cdot I_{HV}) / (I_{VV} \cdot I_{HH} + 2I_{VH} \cdot I_{HV})$$

The correct alignment of the polarizers was verified using a diluted colloidal silica suspension ( $r \geq 0.97$ ).

**Native Chemical Ligation Reaction on PA-Coated Surfaces and Microparticles.** All PAs, peptides, and other materials were UV-sterilized prior to use to maintain sterility. 12 mm glass coverslips were coated with 0.01% poly(D-lysine) (PDL) overnight and then washed with water and dried overnight. The PDL-coated coverslips were then coated with 0.25% alginate dissolved in water for 1 h, after which the alginate was cross-linked with 10 mM calcium chloride in water. The alginate-coated coverslips were then coated with 0.5 mM PA dissolved in water with 5 equiv DTT overnight. Alginate microparticles were similarly coated with 0.5 mM PA dissolved in water with 5 equiv DTT for 30 min. Following wash steps with water and PBS, the PA-coated coverslips or microparticles were immersed in NCL solution, which contained either 0.5 mM peptide-Nbz or 5  $\mu$ M YFP-MESNA and 5  $\mu$ M CFP-MESNA dissolved in PBS with 5 equiv of 4-MPAA and DTT. Following a 24 h incubation at 37 °C, the coverslips or microparticles were washed with PBS, and the coverslips were either used for cell morphology and viability studies or assayed for YFP fluorescence on a SpectraMax MS microplate reader, while the microparticles were visualized by confocal microscopy for both YFP and CFP fluorescence.

**Cell Culture.** NIH/3T3 mouse embryonic fibroblasts (American Type Culture Collection, Manassas, VA) were maintained in monolayer culture in T25 culture flasks. Growth medium consisted of Dulbecco's Modified Eagle Medium (DMEM) with high glucose supplemented with 10% fetal bovine serum, 100 U/mL penicillin, and 100  $\mu$ g/mL streptomycin. Assay medium consisted of growth medium without serum.

**Cell Morphology and Viability Assays.** The PA-coated coverslips functionalized using the NCL reaction were placed in 24-well plates and seeded with 5,000 NIH/3T3 fibroblasts in 1 mL assay medium per well. Following a 5 h incubation at 5% CO<sub>2</sub> and 37 °C, the coverslips were washed with PBS containing 1 mM CaCl<sub>2</sub> and fixed for subsequent analysis.

For quantification of cell spreading, fibroblasts were stained with phalloidin and visualized by light microscopy. Coverslips were fixed in 4% paraformaldehyde in PBS for 30 min at room temperature, then blocked with blocking buffer (10% normal goat serum, 2% bovine serum albumin, and 0.4% Triton X100) for 30 min at 4 °C, then stained for F-actin with rhodamine-phalloidin (Invitrogen, Grand Island, NY) at 1:500 dilution for 2 h at room temperature, and finally dried and mounted on slides for light microscopy. Solutions used in fixing, staining, and washing steps were supplemented with 1 mM CaCl<sub>2</sub> to maintain alginate cross-linking. The cells were imaged using a Nikon Eclipse TE2000-U inverted fluorescence microscope, and images were analyzed using the Shape Descriptor 1u plugin on ImageJ software (NIH) to determine the circularity of the cells (calculated as  $4\pi \times \text{area}/\text{perimeter}^2$ ).

Cell viability was assessed using commercially available LIVE/DEAD cell viability assay kit (Life Technologies). Fibroblasts were cultured on PA coating for 5 h and stained with 1 µg/mL calcein AM and 1 µg/mL ethidium homodimer-1 following manufacturer's protocol. Live cell (calcein positive) and dead cell (ethidium homodimer positive) populations were counted manually under an inverted fluorescence microscope (Nikon Eclipse TE2000-U).

**Statistics and Data Analysis.** For the determination of form factor, five images from each of two replicates of each condition were analyzed, and the mean and standard deviation of the form factor of cells were calculated across all ten images. To establish statistical significance, each condition was compared to CysPA alone using the Student's *t* test. For comparison of cell viability approximately 100 cells were counted from at least two replicates per condition. The cell viability index was defined as the ratio of calcein positive cells to the total number of cells. Statistical significance was measured against CysPA alone. For the determination of YFP fluorescence on PA coatings, two independent measurements of the fluorescence emission at 535 nm following excitation at 495 nm were taken from each of four replicates of each condition, and the mean and standard error were calculated based on these four replicates for each condition following background subtraction of wells with alginate-coated coverslips without PA nanofibers. To establish statistical significance, the CysPA-YFP NCL condition was compared to each control using the Student's *t* test. For the statistical comparison of fluorescence anisotropy, three independent replicates were measured for each condition, and the CysPA condition was compared to the GlyPA and YFP only conditions using the Student's *t* test.

## ■ ASSOCIATED CONTENT

### Supporting Information

Description of the construction of the expression plasmids for EYFP-MESNA and ECFP-MESNA is provided in Methods. A detailed mechanism for the NCL reaction and confirmation of this mechanism by mass spectroscopy is provided in Figure 1. CD spectra of PAs with analysis of secondary structure analysis is provided in Figure 2. A schematic of the protocol for coating surfaces with PA nanofibers for assessment of cell adhesion and spreading is provided in Figure 3. The cell viability on PA coatings is provided in Figure 4. The structure of the TAMRA-labeled PA, full pictures of the protein gels, and a full field of the fluorescent protein-ligated PA-coated microparticles are shown in Figure 5. This material is available free of charge via the Internet at <http://pubs.acs.org>.

## ■ AUTHOR INFORMATION

### Corresponding Author

\*E-mail: s-stupp@northwestern.edu; Phone 312-503-0807.

### Present Address

Patricia Y. W. Yankers and Ricardo M. P. da Silva, Institute for Complex Molecular Systems, Eindhoven University of Technology Den Dolech 2, 5612 AZ Eindhoven, Netherlands; +31 (0)40 247 9111, m.r.da.silva@tue.nl, p.y.w.dankers@tue.nl

### Notes

The authors declare no competing financial interest.

## ■ ACKNOWLEDGMENTS

This work was funded by a grant from the National Institutes of Health—National Institute of Biomedical Imaging and Bioengineering (2 R01 EB003806-06A2, NIH/NIBIB). S.K. acknowledges support from the National Institutes of Health—National Institute on Drug Abuse (5 T90 DA022881 NIH/NIDA). P.Y.W.D. acknowledges the Council for Chemical Sciences of The Netherlands Organization for Scientific Research (CW-NWO) and J.B. acknowledges the NWO for a Rubicon grant. The authors would like to acknowledge the following core facilities at Northwestern University: Cell Imaging Facility, Electron Probe Instrumentation Center and Institute for BioNanotechnology and Medicine. Finally, the authors would like to thank Xuan Yue for performing the LC-MS analysis, Liam Palmer for editing this manuscript, Marieke Rensen, Maarten Merkx, and Joost van Dongen for their input with respect to the fluorescent protein experiments and Mark Seniw for graphic designs used in this contribution.

## ■ REFERENCES

- Petty, R. T., Li, H. W., Maduram, J. H., Ismagilov, R., and Mrksich, M. (2007) Attachment of cells to islands presenting gradients of adhesion ligands. *J. Am. Chem. Soc.* 129 (29), 8966–8967.
- Engler, A. J., Sweeney, H. L., Discher, D. E., and Schwarzbauer, J. E. (2007) Extracellular matrix elasticity directs stem cell differentiation. *J. Musculoskeletal Neuronal Interact.* 7 (4), 335.
- Gilbert, P. M., Havenstrite, K. L., Magnusson, K. E., Sacco, A., Leonardi, N. A., Kraft, P., Nguyen, N. K., Thrun, S., Lutolf, M. P., and Blau, H. M. (2010) Substrate elasticity regulates skeletal muscle stem cell self-renewal in culture. *Science* 329 (5995), 1078–1081.
- Kim, B. S., and Mooney, D. J. (1998) Development of biocompatible synthetic extracellular matrices for tissue engineering. *Trends Biotechnol.* 16 (5), 224–230.
- Fields, G. B., Lauer, J. L., Dori, Y., Forns, P., Yu, Y. C., and Tirrell, M. (1998) Protein-like molecular architecture: biomaterial applications for inducing cellular receptor binding and signal transduction. *Biopolymers* 47 (2), 143–51.
- Ghanaati, S., Webber, M. J., Unger, R. E., Orth, C., Hulvat, J. F., Kiehna, S. E., Barbeck, M., Rasic, A., Stupp, S. I., and Kirkpatrick, C. J. (2009) Dynamic *in vivo* biocompatibility of angiogenic peptide amphiphile nanofibers. *Biomaterials* 30 (31), 6202–6212.
- (a) Hartgerink, J. D., Beniash, E., and Stupp, S. I. (2001) Self-assembly and mineralization of peptide-amphiphile nanofibers. *Science* 294 (5547), 1684–1688. (b) Hartgerink, J. D., Beniash, E., and Stupp, S. I. (2002) Peptide-amphiphile nanofibers: a versatile scaffold for the preparation of self-assembling materials. *Proc. Natl. Acad. Sci. U.S.A.* 99 (8), 5133–5138.
- (a) Palmer, L. C., and Stupp, S. I. (2008) Molecular self-assembly into one-dimensional nanostructures. *Acc. Chem. Res.* 41 (12), 1674–1684. (b) Palmer, L. C., Velichko, Y. S., de la Cruz, M. O., and Stupp, S. I. (2007) Supramolecular self-assembly codes for functional structures. *Philos. Trans. R. Soc., A* 365 (1855), 1417–1433. (c) Paramonov, S. E., Jun, H.-W., and Hartgerink, J. D. (2006) Self-assembly of peptide-amphiphile nanofibers: the roles of hydrogen

- bonding and amphiphilic packing. *J. Am. Chem. Soc.* 128 (22), 7291–7298. (d) Tovar, J. D., Claussen, R. C., and Stupp, S. I. (2005) Probing the interior of peptide amphiphile supramolecular aggregates. *J. Am. Chem. Soc.* 127 (20), 7337–7345. (e) Velichko, Y. S., Stupp, S. I., and de la Cruz, M. O. (2008) Molecular simulation study of peptide amphiphile self-assembly. *J. Phys. Chem. B* 112 (8), 2326–2334.
- (9) (a) Pashuck, E. T., Cui, H., and Stupp, S. I. (2010) Tuning supramolecular rigidity of peptide fibers through molecular structure. *J. Am. Chem. Soc.* 132 (17), 6041–6046. (b) Greenfield, M. A., Hoffman, J. R., de la Cruz, M. O., and Stupp, S. I. (2010) Tunable mechanics of peptide nanofiber gels. *Langmuir* 26 (5), 3641–3647. (c) Newcomb, C. J., Sur, S., Ortony, J. H., Lee, O. S., Matson, J. B., Boekhoven, J., Yu, J. M., Schatz, G. C., and Stupp, S. I. (2014) Cell death versus cell survival instructed by supramolecular cohesion of nanostructures. *Nat. Commun.* 5, 3321.
- (10) (a) Malkar, N. B., Lauer-Fields, J. L., Juska, D., and Fields, G. B. (2003) Characterization of peptide-amphiphiles possessing cellular activation sequences. *Biomacromolecules* 4 (3), 518–528. (b) Mardilovich, A., Craig, J. A., McCammon, M. Q., Garg, A., and Kokkoli, E. (2006) Design of a novel fibronectin-mimetic peptide-amphiphile for functionalized biomaterials. *Langmuir* 22 (7), 3259–3264. (c) Rajangam, K., Arnold, M. S., Rocco, M. A., and Stupp, S. I. (2008) Peptide amphiphile nanostructure-heparin interactions and their relationship to bioactivity. *Biomaterials* 29 (23), 3298–3305. (d) Rajangam, K., Behanna, H. A., Hui, M. J., Han, X., Hulvat, J. F., Lomasney, J. W., and Stupp, S. I. (2006) Heparin binding nanostructures to promote growth of blood vessels. *Nano Lett.* 6 (9), 2086–2090. (e) Shah, R. N., Shah, N. A., Del Rosario Lim, M. M., Hsieh, C., Nuber, G., and Stupp, S. I. (2010) Supramolecular design of self-assembling nanofibers for cartilage regeneration. *Proc. Natl. Acad. Sci. U.S.A.* 107 (8), 3293–3298. (f) Boekhoven, J., and Stupp, S. I. (2014) Supramolecular materials for regenerative medicine. *Adv. Mater.* 26 (11), 1642–1659.
- (11) Guler, M. O., Soukasene, S., Hulvat, J. F., and Stupp, S. I. (2005) Presentation and recognition of biotin on nanofibers formed by branched peptide amphiphiles. *Nano Lett.* 5 (2), 249–252.
- (12) (a) Behanna, H. A., Donners, J. J. J. M., Gordon, A. C., and Stupp, S. I. (2005) Coassembly of amphiphiles with opposite peptide polarities into nanofibers. *J. Am. Chem. Soc.* 127 (4), 1193–1200. (b) Behanna, H. A., Rajangam, K., and Stupp, S. I. (2007) Modulation of fluorescence through coassembly of molecules in organic nanostructures. *J. Am. Chem. Soc.* 129 (2), 321–327. (c) Niece, K. L., Hartgerink, J. D., Donners, J. J. J. M., and Stupp, S. I. (2003) Self-assembly combining two bioactive peptide-amphiphile molecules into nanofibers by electrostatic attraction. *J. Am. Chem. Soc.* 125 (24), 7146–7147.
- (13) Silva, G. A., Czeisler, C., Niece, K. L., Beniash, E., Harrington, D. A., Kessler, J. A., and Stupp, S. I. (2004) Selective differentiation of neural progenitor cells by high-epitope density nanofibers. *Science* 303 (5662), 1352–1355.
- (14) Webber, M., Tongers, J., Renault, M., Roncalli, J., Losordo, D., and Stupp, S. (2009) Development of bioactive peptide amphiphiles for therapeutic cell delivery. *Acta Biomater.* 6 (1), 3–11.
- (15) Storrie, H., Guler, M. O., Abu-Amara, S. N., Volberg, T., Rao, M., Geiger, B., and Stupp, S. I. (2007) Supramolecular crafting of cell adhesion. *Biomaterials* 28 (31), 4608–4618.
- (16) Webber, M. J., Tongers, J., Newcomb, C. J., Marquardt, K. T., Bauersachs, J., Losordo, D. W., and Stupp, S. I. (2011) Supramolecular nanostructures that mimic VEGF as a strategy for ischemic tissue repair. *Proc. Natl. Acad. Sci. U.S.A.* 108 (33), 13438–13443.
- (17) Khan, S., Sur, S., Newcomb, C. J., Appelt, E. A., and Stupp, S. I. (2012) Self-assembling glucagon-like peptide 1-mimetic peptide amphiphiles for enhanced activity and proliferation of insulin-secreting cells. *Acta Biomater.* 8 (5), 1685–1692.
- (18) Goldberger, J. E., Berns, E. J., Bitton, R., Newcomb, C. J., and Stupp, S. I. (2011) Electrostatic control of bioactivity. *Angew. Chem., Int. Ed. Engl.* 50 (28), 6292–6295.
- (19) (a) Dawson, P. E., Muir, T. W., Clark-Lewis, I., and Kent, S. B. (1994) Synthesis of proteins by native chemical ligation. *Science* 266 (5186), 776–779. (b) Dawson, P. E., and Kent, S. B. (2000) Synthesis of native proteins by chemical ligation. *Annu. Rev. Biochem.* 69, 923–960.
- (20) Blanco-Canosa, J. B., and Dawson, P. E. (2008) An efficient Fmoc-SPPS approach for the generation of thioester peptide precursors for use in native chemical ligation. *Angew. Chem., Int. Ed. Engl.* 47 (36), 6851–6855.
- (21) Franke, R., Doll, C., and Eichler, J. (2005) Peptide ligation through click chemistry for the generation of assembled and scaffolded peptides. *Tetrahedron Lett.* 46 (26), 4479–4482.
- (22) Jung, J. P., Jones, J. L., Cronier, S. A., and Collier, J. H. (2008) Modulating the mechanical properties of self-assembled peptide hydrogels via native chemical ligation. *Biomaterials* 29 (13), 2143–2151.
- (23) Byun, E., Kim, J., Kang, S. M., Lee, H., Bang, D., and Lee, H. (2011) Surface PEGylation via native chemical ligation. *Bioconjugate Chem.* 22 (1), 4–8.
- (24) Long, L., Lin, W., Chen, B., Gao, W., and Yuan, L. (2011) Construction of a FRET-based ratiometric fluorescent thiol probe. *Chem. Commun.* 47 (3), 893–895.
- (25) Hu, B. H., Su, J., and Messersmith, P. B. (2009) Hydrogels cross-linked by native chemical ligation. *Biomacromolecules* 10 (8), 2194–2200.
- (26) (a) Reulen, S. W. A., Brusselaars, W. W. T., Langereis, S., Mulder, W. J. M., Breurken, M., and Merkx, M. (2007) Protein-liposome conjugates using cysteine-lipids and native chemical ligation. *Bioconjugate Chem.* 18 (2), 590–596. (b) Reulen, S. W. A., van Baal, I., Raats, J. M. H., and Merkx, M. (2009) Efficient, chemoselective synthesis of immunomicelles using single-domain antibodies with a C-terminal thioester. *BMC Biotechnol.* 9, 66. (c) Venter, P. A., Dirksen, A., Thomas, D., Manchester, M., Dawson, P. E., and Schneemann, A. (2011) Multivalent display of proteins on viral nanoparticles using molecular recognition and chemical ligation strategies. *Biomacromolecules* 12 (6), 2293–2301.
- (27) Ruoslahti, E., and Pierschbacher, M. D. (1987) New perspectives in cell-adhesion - Rgd and Integrins. *Science* 238 (4826), 491–497.
- (28) Massia, S. P., and Hubbell, J. A. (1991) An RGD spacing of 440 nm is sufficient for integrin alpha V beta 3-mediated fibroblast spreading and 140 nm for focal contact and stress fiber formation. *J. Cell Biol.* 114 (5), 1089–1100.
- (29) Sur, S., Matson, J. B., Webber, M. J., Newcomb, C. J., and Stupp, S. I. (2012) Photodynamic control of bioactivity in a nanofiber matrix. *ACS Nano* 6 (12), 10776–10785.
- (30) Grafahrend, D., Heffels, K. H., Beer, M. V., Gasteier, P., Moller, M., Boehm, G., Dalton, P. D., and Groll, J. (2011) Degradable polyester scaffolds with controlled surface chemistry combining minimal protein adsorption with specific bioactivation. *Nat. Mater.* 10 (1), 67–73.
- (31) Boekhoven, J., Rubert Perez, C. M., Sur, S., Worthy, A., and Stupp, S. I. (2013) Dynamic display of bioactivity through host-guest chemistry. *Angew. Chem., Int. Ed. Engl.* 52 (46), 12077–12080.
- (32) Sung, K. E., Yang, N., Pehlke, C., Keely, P. J., Eliceiri, K. W., Friedl, A., and Beebe, D. J. (2011) Transition to invasion in breast cancer: a microfluidic in vitro model enables examination of spatial and temporal effects. *Integr. Biol.* 3 (4), 439–450.
- (33) Schwartzman, M., Palma, M., Sable, J., Abramson, J., Hu, X., Sheetz, M. P., and Wind, S. J. (2011) Nanolithographic control of the spatial organization of cellular adhesion receptors at the single-molecule level. *Nano Lett.* 11 (3), 1306–1312.
- (34) (a) Shi, Y., Mowery, R. A., Ashley, J., Hentz, M., Ramirez, A. J., Bilgicer, B., Slunt-Brown, H., Borchelt, D. R., and Shaw, B. F. (2012) Abnormal SDS-PAGE migration of cytosolic proteins can identify domains and mechanisms that control surfactant binding. *Protein Sci.* 21 (8), 1197–1209. (b) Khosravi-Far, R., Lutz, R. J., Cox, A. D., Conroy, L., Bourne, J. R., Sinensky, M., Balch, W. E., Buss, J. E., and Der, C. J. (1991) Isoprenoid modification of rab proteins terminating in CC or CXC motifs. *Proc. Natl. Acad. Sci. U.S.A.* 88 (14), 6264–6268.

- (35) Lau, C., Bitton, R., Bianco-Peled, H., Schultz, D. G., Cookson, D. J., Grosser, S. T., and Schneider, J. W. (2006) Morphological characterization of self-assembled peptide nucleic acid amphiphiles. *J. Phys. Chem. B* 110 (18), 9027–9033.
- (36) Vaknin, A., and Berg, H. C. (2008) Direct evidence for coupling between bacterial chemoreceptors. *J. Mol. Biol.* 382 (3), 573–577.
- (37) Soukasene, S., Toft, D. J., Moyer, T. J., Lu, H., Lee, H. K., Standley, S. M., Cryns, V. L., and Stupp, S. I. (2011) Antitumor activity of peptide amphiphile nanofiber-encapsulated camptothecin. *ACS Nano* 5 (11), 9113–9121.
- (38) Sambrook, J.; Russell, D. W. *Molecular Cloning - A laboratory manual*; Cold Spring Harbor Laboratory Press: New York, 2001.
- (39) Reed, J., and Reed, T. A. (1997) A set of constructed type spectra for the practical estimation of peptide secondary structure from circular dichroism. *Anal. Biochem.* 254 (1), 36–40.